Theor Chem Acc (2011) 130:15–25
DOI 10.1007/s00214-011-0952-6

REGULAR ARTICLE

On the catalytic mechanism of $Pt_4^{+/-}$ in the oxygen transport activation of N_2O by CO

Lingling Lv · Yongcheng Wang · Yanzhi Jin

Received: 28 December 2010 / Accepted: 26 April 2011 / Published online: 8 May 2011

Abstract The two-state reaction mechanism of the $Pt_4^{+/-}$ with N_2O (CO) on the quartet and doublet potential energy surfaces has been investigated at the B3LYP level. The effect of Pt_4^- anion assistance is analyzed using the activation strain model in which the activation energy ($\Delta E^{\neq}$) is decomposed into the distortion energies ($\Delta E^{\neq}_{\text{dist}}$) and the stabilizing transition state (TS) interaction energies ($\Delta E^{\neq}_{\text{int}}$), namely $\Delta E^{\neq} = \Delta E^{\neq}_{\text{dist}} + \Delta E^{\neq}_{\text{int}}$. The lowering of activation barriers through Pt_4^- anion assistance is caused by the TS interaction $\Delta E^{\neq}_{\text{int}}$ (−90.7 to −95.6 kcal/mol) becoming more stabilizing. This is attributed to the N_2O π*-LUMO and Pt d HOMO back-donation interactions. However, the strength of the back-donation interactions has significantly impact on the reaction mechanism. For the Pt_4^- anion system, it has very significant back-bonding interaction (N_2O negative charge of 0.79e), HOMO has 81.5% π* LUMO(N_2O) character, with 3d orbital contributions of 10.7% from $Pt_{(3)}$ and 7.7% from $Pt_{(7)}$ near the ^{4}TS4 transition state. This facilitates the bending of the N_2O molecule, the N–O bond weakening, and an $O^-(^2P)$ dissociation without surface crossing. For the Pt_4^+ cation system, the strength of the charge transfer is weaker, which leads to the diabatic (spin conserving) dissociation of N_2O: $N_2O(^1\sum^+) \rightarrow N_2(^1\sum_g^+) + O(^1D)$. The quartet to doublet state transition should occur efficiently near the ^{4}TS1 due to the larger SOC value calculated of 677.9 cm^{-1}. Not only will the reaction overcome spin-change-induced barrier (ca. 7 kcal/mol) but also overcome adiabatic barrier (ca. 40.1 kcal/mol).Therefore, the lack of a thermodynamic driving force is an important factor contributing to the low efficiency of the reaction system.

Keywords $Pt_4^{+/-}$ and N_2O · Activation strain model · Back-donation Interaction · Spin–orbit coupling (SOC)

1 Introduction

N_2O is one of the greenhouse gases, and its impact toward the environment is even more negative than CO_2 and methane effects due to its persistence and stable in the atmosphere for about 130 years. Recently, there has been considerable concern about environmental issues associated with the growth of the N_2O concentration in atmosphere as a result of human activity [1], and in this global context, considerable efforts have been devoted to find ways of reducing anthropogenic emission of greenhouse nitrous oxide gas. Thus, the activation and cleavage of N_2O is one of the challenging subjects of academic research because they can provide fundamental information about catalytic bond activation. A large number of recent studies both experimental and theoretical have been devoted to the reactions of gas-phase transition metal atoms or ions with N_2O [2–14], which is well understood and studied. Three different mechanisms [15] have been proposed to account for the observed features of the kinetics: the surface-crossing model

Electronic supplementary material The online version of this article (doi:10.1007/s00214-011-0952-6) contains supplementary material, which is available to authorized users.

L. Lv · Y. Wang (✉) · Y. Jin
Gansu Key Laboratory of Polymer Materials,
College of Chemistry and Chemical Engineering,
Northwest Normal University, 805 N Anning East Road,
Lanzhou, Gansu 730070, China
e-mail: lvling100@163.com

L. Lv
College of Life science and Chemistry,
Tianshui Normal University, Tianshui, Gansu 741001, China

(also called the direct abstraction mechanism), the electron-transfer (ET) mechanism, and the resonance interaction model.

The subject of small molecules activated processes via metal cluster has also attracted much attention of theoreticians and experimentalists in the past decade [16–19]. One of the motivations for these studies is the insight cluster reactions can provide into the mechanism of reactions on metal surfaces, especially those related to catalytic processes. The gas-phase reaction $N_2O + CO \rightarrow CO_2 + N_2$ is quite exothermic by 87.3 kcal/mol, and they do not occur directly to any measurable extent in the gas phase at either room or elevated temperatures [20, 21]. The first gas-phase catalysis reactions of this type were reported by Kappes and Staley [22], who showed that atomic Fe^+ cation catalyzes the $N_2O + CO \rightarrow CO_2 + N_2$ reaction via a FeO^+ intermediate. Bohme and co-workers [20, 21] have recently observed similar catalytic process by using inductively coupled plasma/selected-ion flow tube (ICP/SIFT) tandem mass spectrometry for 26 atomic cations. The results show that catalytic activity is observed with only 10 of these 26 atomic cations, namely Pt^+, Ca^+, Fe^+, Ge^+, Sr^+, Ba^+, Os^+, Ir^+, Eu^+, and Y^+. Atomic Pt^+ has also been shown to mediate the reaction of N_2O and CO efficiently, with $k = 7 \times 10^{-11}$ for the reduction of N_2O and 6.7×10^{-10} cm^3 $molecule^{-1}$ s^{-1} for the oxidation of CO. The corresponding theoretical studies were performed by Russo [23] and our groups [24]. The reactions of the positively charged clusters Pt_n^+ ($n = 1$–5) activate N_2O were investigated using a FT-ICR mass spectrometry by Koszinowski, Schröder and Schwarz [25]. With respect to thermodynamics, the reactions (see Scheme 1) are highly favorable because both a relatively strong metal-oxide bond is formed and the particularly stable N_2 molecule is released. However, the rate constants actually observed for the primary reaction are rather low for the different cluster sizes examine. For Pt_4^+, bimolecular rate constant is $k \leq 3.0 \times 10^{-13}$ cm^3 s^{-1}, efficiency for $\varphi \leq 5.0 \times 10^{-4}$, which shows that the occurrence of reactions could not be established at all. Conversely, early experimental studies by Ervin and co-workers [26, 27] demonstrated that platinum cluster anions Pt_n^- ($n = 3$–7) efficiently catalyze the oxidation of CO to CO_2 by N_2O or O_2. The reactions are exothermic and occur at approximately room temperature

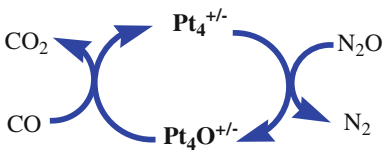

Scheme 1 N2O activation cycle by CO in the presence of Pt4$^{+/-}$ catalysts

with no appreciable activation barrier (<1 kcal/mol at 300 K). For example, the $Pt_4^- + N_2O \rightarrow Pt_4O^- + N_2$ reaction, bimolecular rate constant is $k = 3.4 \pm 0.1 \times 10^{-10}$ cm^3 s^{-1} for the reduction of N_2O, while the efficiency of the $Pt_4O^- + CO \rightarrow Pt_4^- + CO_2$ reaction is $\varphi = 0.76 \pm 0.11$ for the oxidation of CO. Recently, Pt_4^- catalyzes the conversion of CO and N_2O to CO_2 and N_2 in the gas phase, as observed by Siu and co-workers [26, 27] using Fourier transform ion cyclotron (FT-ICR) mass spectrometry. The results show that Pt_4^- is a very active catalyst for the conversion of CO to CO_2 with N_2O, while Pt_4^+ reacts only with slow addition of CO. Thus, we must ask why efficiency of the $Pt_4^- + N_2O \rightarrow Pt_4O^- + N_2$ reaction is much higher than that of Pt_4^+ and N_2O. This is the motivation to investigate the title reactions.

However, the chemistry of transition metals and their cluster compounds is strongly influenced by the availability of multiple low-lying electronic states in these species [28–30]. This means that the reactions involving several electronic states that may also have different spins should involve spin-conserving and spin inversion processes. Thus, a reaction possibly occurs on two or more potential energy surfaces (PESs) under thermal conditions, and therefore, it has to involve the electronic process of radiationless transition from one potential energy surface to another surface. In this case, the changes between two or more different electronic states are known to accompany the progress of the reaction and can modify the efficiency and/or selectivity of a given chemical rearrangement and can also influence a reaction from a process without change in spin state to a situation where the spin change completely determines the rate and selectivity [31–35].

Therefore, detailed analyses of crossing seam between the different potential energy surfaces are important in order to better understand the mechanism of the title reactions. Our motivation is to facilitate an understanding of the role of electronic structures on mechanistic details at a molecular level. This kind of knowledge is essential for understanding the whole reaction mechanism and is useful for establishing an appropriate model for the N–O cleavage process. To our knowledge, a deep theoretical study for the catalytic mechanism of $Pt_4^{+/-}$ in the oxygen transport activation of N_2O by CO has not been reported. In present paper, to understand the factors controlling of the title reactions, we have analyzed the three model reactions using the activation strain model [36, 37] in which the activation energy ($\Delta E^{\neq}$) is decomposed into the distortion energies ($\Delta E^{\neq}_{dist}$) and the stabilizing transition state (TS) interaction energies ($\Delta E^{\neq}_{int}$), namely $\Delta E^{\neq} = \Delta E^{\neq}_{dist} + \Delta E^{\neq}_{int}$. We also discussed crossing point of the quartet and doublet PESs, spin–orbit coupling (SOC), and possible spin inversion processes in this intriguing chemical reaction.

The two N–O bond activation of N_2O are carried out a detailed analysis of electronic structure.

2 Computational details

2.1 Geometry optimization

Computations were carried out using the Gaussian 03 ab initio program package [38]. Energies and geometries of the reaction intermediates and the transition states were calculated with DFT using the B3LYP level. Unrestricted wave functions were used for all open-shell species. The double-zeta 6-31++G(d, p) basis set of Pople and co-workers [39] was used for N and O, and the standard effective core potential (ECP) LanL2DZ together with the associated (8s6p3d) primitive set [40, 41] resulting in a (341|321|21)[3s3p2d] contraction was used to describe the 5s, 5p, 5d, and 6s electrons on platinum. To further examine the effect of the choice of basis sets, single-point calculations using the structural data obtained from the B3LYP calculations for all of the reactants, intermediates, transition states, and products were performed using the 6–311++G(d, p) basis set for N and O, and the (8s7p6d) primitive set of the standard Stuttgart/Dresden effective core potential (ECP) SDD, resulting in a (311111|31111|411)[6s5p3d] contraction [42], was used for $Pt_4^{+/-}$. Previous investigations of transition metal compounds employing the B3LYP functional by other groups [43–45] and us [46–48] indicated that this approach shows a very promising performance to predict properties such as bond dissociation energies, geometries, and harmonic frequencies with an accuracy comparable to that obtained from highly correlated wave function-based ab initio methods.

All stationary points were characterized by vibrational analysis, and the zero-point energy (ZPE) was calculated. The transition state structures all represent saddle points, characterized by one negative eigenvalue of the Hessian matrix. The intrinsic reaction coordinate (IRC) was then calculated and used to track the minimum energy path from transition states to the corresponding minima, to probe the reaction path and check whether the correct transition state was located.

To locate the crossing seam between the two PESs of different spin states, we have carried out single-point energy calculations (in the quartet state) as a function of the structural change along the IRC of the doublet state [49, 50]: in this way, we have obtained the crossing point (CP). The natural bond orbital (NBO) and natural resonance theory (NRT) analyses were also carried out using the NBO 5.0 procedure [51].

2.2 Spin–orbit coupling calculations

Nonadiabatic coupling of the PESs of different spin states at the CPs and transition states was studied by computing the spin–orbit coupling(SOC) constants using the approximate one-electron spin–orbit Hamiltonian [52, 53] given in Eq. 1:

$$H_{\mathrm{SO}} = \frac{\alpha^2}{2}\sum_i \sum_k \left(\frac{Z_k^*}{r_{ik}^3}\right)(S_i \cdot L_{ik}) = \sum_i h_i(Z^*)\frac{\alpha^2}{2} = \frac{e^2 h}{4\pi m_e^2 c^2} \quad (1)$$

in which the neglect of the two-electron terms is compensated by introducing a semi-empirical parameter; here, the effective nuclear charge is (Z_{eff}). L_{ik} and S_i are the orbital and spin angular momentum operators for electron i in the framework of the nuclei indexed k, respectively, and Z_k^* is the effective nuclear charge.

The root-mean-squared value of the SOC constant is defined as Eq. 2.

$$\mathrm{SOC} = \left(\sum_{M_s=\pm\frac{3}{2},\pm\frac{1}{2}} \sum_{k=x,y,z} \left\langle {}^4\psi(M_s)\middle|\hat{H}_{\mathrm{SO}}\right|^2 \psi(M_s)\rangle_k\right)^{1/2} \quad (2)$$

The SOC constant is relevant to the electronic factor of the rate of the intersystem crossing. The SOC matrix elements in Eq. 2 were evaluated at the doublet/quartet state averaged complete active space self-consistent field [CASSCF (9, 7)] (9 electrons in 7 orbitals) wave function using the SOC-CI method [54]. Since the orbital sets of the doublet and quartet states must share a common set of froze core orbitals to calculate the SOC matrix elements, we employed the wave function of the quartet state as a reference state for doublet CI wave function as well as the quartet one. For the qualitative interpretation of nonzero SOC interaction, we also used ROHF orbitals [55] generated at the quartet state as orbitals from which CASCI wave functions are constructed. All SOC calculations were performed with the GAMESS program package [56].

3 Results and discussion

The optimized geometries along the reaction surfaces are depicted in Fig. 1, and energetic data are listed in Table S1 (see the Supporting Information). In order to keep the discussion more simple, each species is represented with its spin multiplicity as a superscript preceding the formula without its spatial symmetry, respectively. The calculated potential energy profiles for the quartet and doublet states are shown in Figs. 2 and 3.

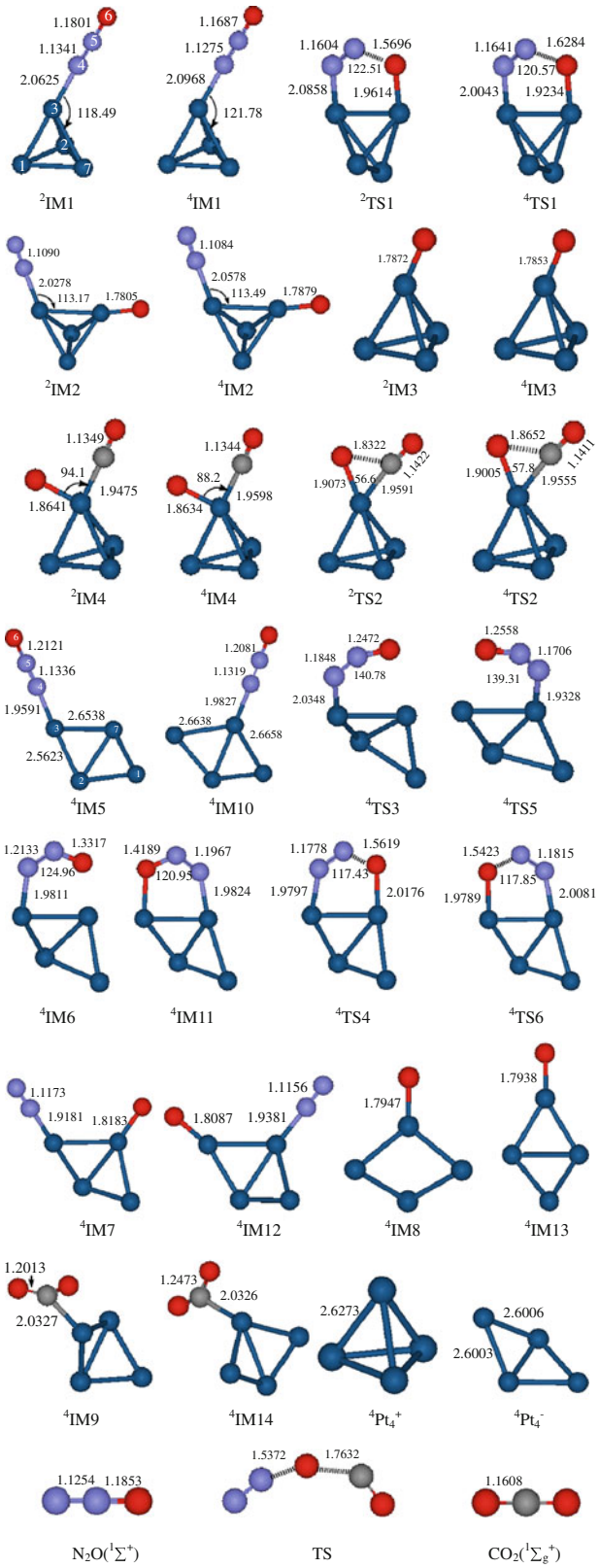

Fig. 1 Optimized structures of transition states and intermediates along the reaction surfaces of the Pt_4^+/Pt_4^- + N2O(CO) systems calculated at the B3LYP/6-31++G(d, p)+LanL2DZ level of theory (bond lengths in angstroms and bond angles in degrees)

3.1 Mechanism of N_2O dissociation

Nitrous oxide is known to have a linear structure in its global energy minimum, characterized by the point symmetry group $C\infty v$ and thus assigned to its $X^1\Sigma^+$ irreducible representation. The N–N bond distance is 1.125 Å (in our theoretical calculation) or 1.128 Å (in experiment), which is between the distances expected for a N–N triple bond (1.098 Å) and a double bond (1.25 Å). The N–O bond distance is 1.185 Å (in our theoretical calculation) or 1.184 Å (in experiment), which is intermediate between the distances expected for a double bond (1.15 Å) and a single bond (∼1.4 Å). This may be characterized by two Lewis resonance structures:

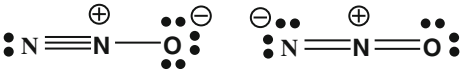

(Weight = 59.7 %) (Weight=34.1%)

The natural resonance theory (NRT) analysis using NBO5.0 [51] shows that resonance weights of the two structures are 59.7 and 34.1%, respectively.

The PESs of the lower-lying electronic states of N_2O were extensively studied by Peyerimhoff and Buenker et al. [57]. In the gas phase, the N–O bond cleavage generates $N_2(X^1\Sigma_g^+)$ and a triplet O atom(^{3}P) in the first elementary step, which is a spin-forbidden dissociation process. The singlet–triplet spin crossover becomes an energetically favorable process and allows N_2O dissociation. According to the multireference configuration interaction (MRCI) calculations [58], the minimum energy crossing point (MECP) on the singlet–triplet intersection corresponds to a linear geometry with a N–O bond distance of 1.787 Å with the energy of 60.3 kcal/mol relative to the global minimum, which has a high reaction barrier due to the spin change.

We also analyzed the reaction path relating to the reduction of N_2O by CO in the absence of any catalyst. The reactive process ($N_2O + CO \rightarrow N_2 + CO_2$) is plotted in Figs. 2 and 3. Our calculations show that the mechanism is characterized by the only activation barrier of 47.2 kcal/mol and is very exothermic by 86.7 kcal/mol. The exothermic value is in agreement with the experimental indication of 87.0 kcal/mol [20, 21].

From the discussion above, they have a high activation barrier for the thermolysis reaction of N_2O, despite the high exothermicity. In N_2O model chemistry, therefore, transition metals are used as activation centers to overcome this reaction barrier by donating electrons to N_2O. The electrons can come either from a single metal center or from two metal centers forming dimeric products.

3.2 Initial complexes

There are numerous computational studies dealing with the structures and the stability of neutral platinum cluster,

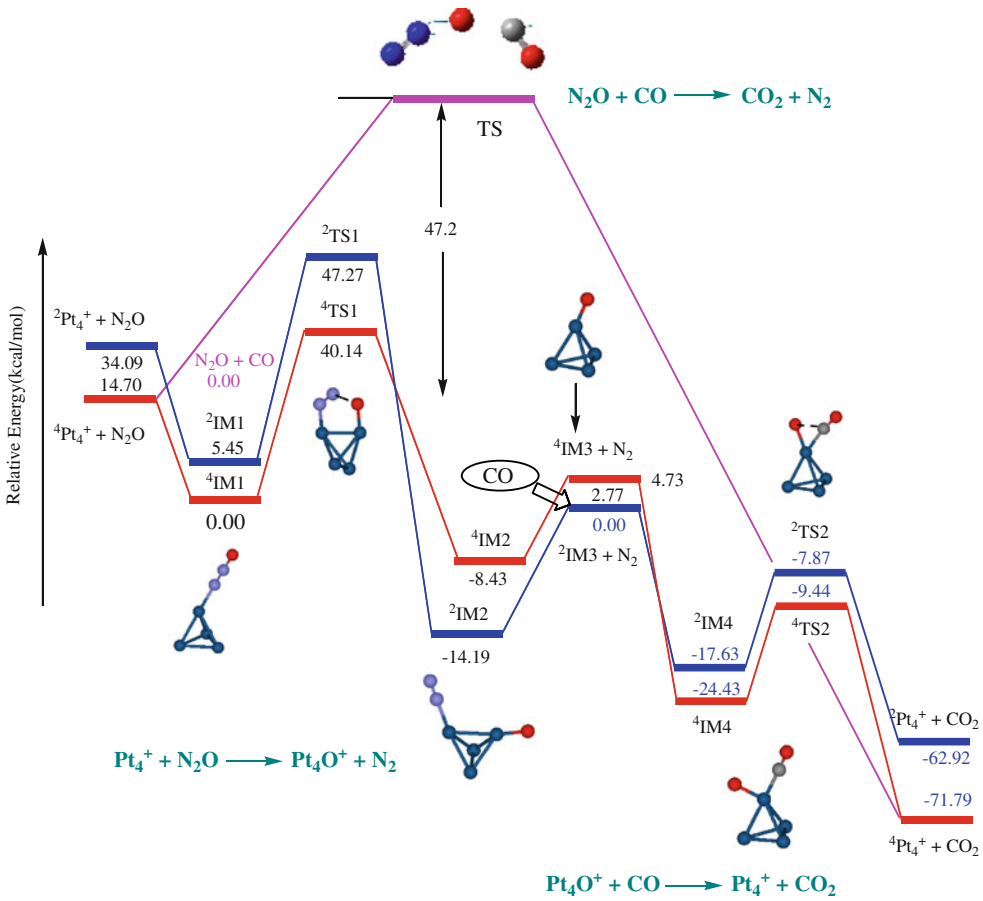

Fig. 2 Potential energy diagram (include zero-point energy) along the doublet and quartet reaction pathway of the $Pt_4^+ + N_2O(CO)$ systems. At the B3LYP/6-31++G(d, p)+LanL2DZ level, relative energies are in kcal/mol. Doublet spin surfaces are indicated by the *blue lines* and quartet spin surfaces by the *red lines*, and the *pink lines* for the $N_2O + CO$ reaction

while there are only a few reports that deal with charged clusters [59]. Possible $Pt_4^{+/-}$ isomers were optimized in both doublet and quartet multiplicities. The ground state of Pt_4^+ corresponds to a quartet, $^4Pt_4^+$ (see Fig. 1), and it has been predicted to be a stable tetrahedral structure in T_d symmetry. The doublet state $^2A''$ has a stable C_s structure ($^2Pt_4^+$), which is less stable than the quartet state $^4Pt_4^+$ by 19.4 kcal/mol. As this energy is very high among the species along the reaction pathway, therefore, detailed analyses of crossing seam between the different potential energy surfaces are important in order to better understand the mechanism of the Pt_4^+ and N_2O reactions. For the anionic Pt_4^- clusters, the ground state of Pt_4^- is predicted to be quartet rhombic structure with a bond length of 2.6 Å (see Fig. 1). The state splitting with the quartet, however, only amounts to 5.2 kcal/mol.

A stabilized reactant-like intermediate, denoted as IM1, is initially formed as $^4Pt_4^{+/-}$ and N_2O collide with each other. We know the frontier molecular orbitals are the main participants in the interactions of the reactants, and the donor/acceptor orbital overlaps dominate the reaction pathway. The molecular orbitals of N_2O show that the N_2O HOMO is a π-orbital, which is antibonding with respect to the O–N bond but bonding to the N–N bond. The LUMO is a π^*-orbital with antibonding character for both the O–N and N–N bonds (46.7% N_t, 33.5% N_c, 19.8% O), which is dominantly terminal N character, and is the electron acceptor orbital for its reduction (see Fig. 4). Thus, for the μ-1,1-N_2O bridging mode possibility, terminal nitrogen coordination configuration is least likely due to the difficulty in oxo-transfer, while terminal μ-1,1-N_2O oxygen coordination has unfavorable $N_2O/Pt_4^{+/-}$ LUMO/HOMO overlap due to the small oxygen contribution in the N_2O LUMO. For the μ-1,3-N_2O bridging mode, the LUMO of N_2O has good overlap with both the $Pt_{(3)}$ d orbital and the $Pt_{(7)}$ orbital in both orientations, which is favorable for electron transfer from $Pt_4^{+/-}$ to N_2O. Therefore, the N_2O ligand can bind in several coordination modes, of which the most stable are a linear end on mode with the terminal nitrogen atom coordinating to $Pt_{(3)}$ and a bent μ-1, 3 bridging mode with the terminal nitrogen atom coordinating to $Pt_{(3)}$ and the oxygen atom coordinating to $Pt_{(7)}$.

Two reaction modes are optimized at the B3LYP/6-31++G(d, p)+LanL2DZ level. In the case of Pt_4^+ cationic clusters, surprisingly, it is failure to optimize the bent μ-1, 3 bridging mode with the terminal nitrogen atom coordinating to $Pt_{(3)}$ and the oxygen atom coordinating to $Pt_{(7)}$. Any such reaction pathway of steepest descent would, in

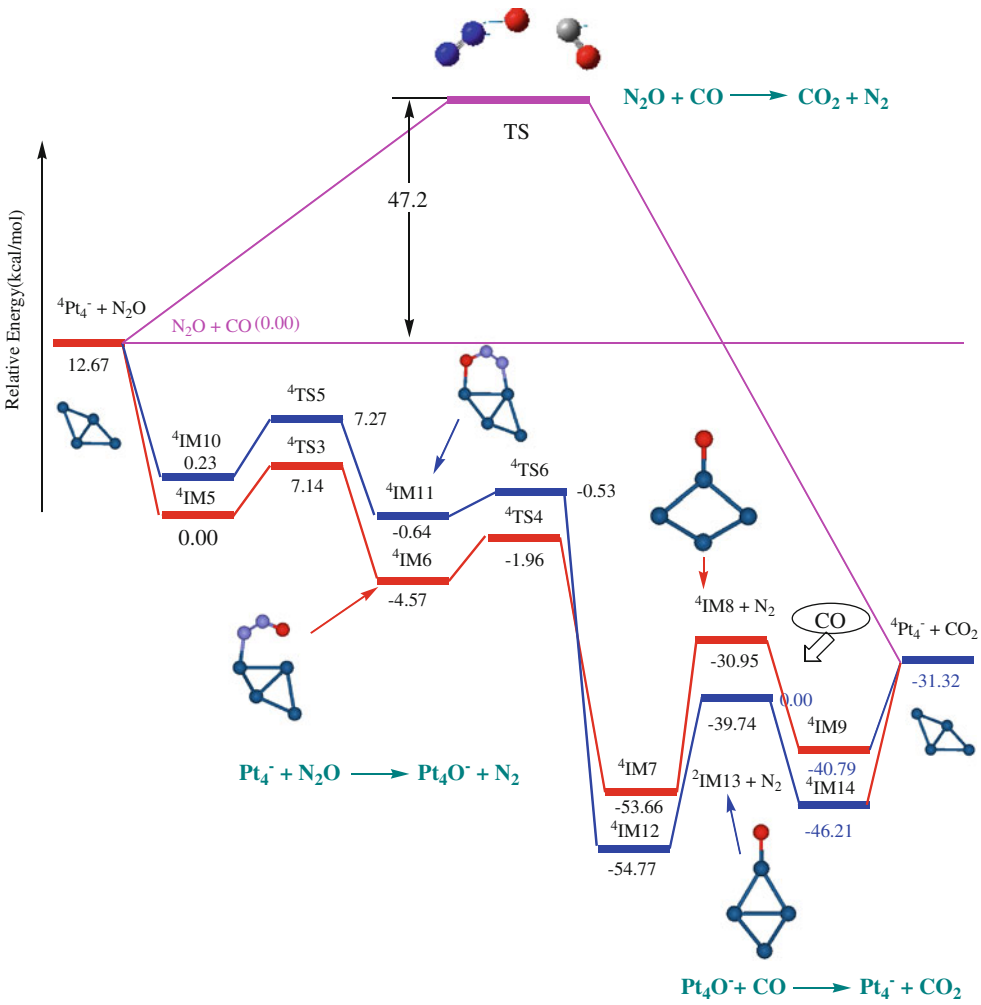

Fig. 3 Potential energy diagram (include zero-point energy) along the quartet reaction pathway of the $Pt_4^- + N_2O$ (CO) systems. At the B3LYP/6-31++G(d, p)+LanL2DZ level, relative energies are in kcal/mol. One pathway is indicated by the *red lines* and the other by the *blue lines*, and the *pink lines* for the $N_2O + CO$ reaction

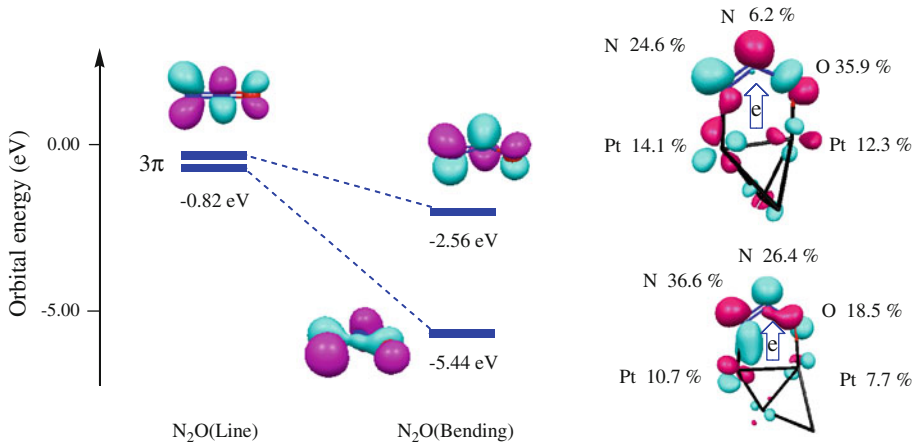

Fig. 4 LUMOs of the linear and bent N_2O molecules and the HOMOs of μ-1,3-bridged $Pt_4^{+/-}$–N_2O complexes

principle, lead to an energy minimum in reactant or product ''valleys'' [60]. Our IRC analysis was, unfortunately, terminated before reaching the true local minimum point for the reactant intermediate (a bent μ-1, 3 bridging modes) since the reaction coordinate changes are taken place from the O–N bond cleavage to ∠PtNN bending. Then, we optimized this point, leading to a stable intermediate, ^{4}IM1 (or ^{2}IM1), formed. These calculated results are shown in Figure S1 (see Supporting Information). As can be seen from Fig. 2, the linear end on mode ^{4}IM1 is predicted to be more stable than the $^4Pt_4^+ + N_2O$ entrance channel by 14.7 kcal/mol due to the ligand–metal weak interactions

and the d-d electron exchange interaction, which favors high-spin situation. For the Pt_4^- anionic clusters, from $Pt_4^- + N_2O$, the reaction splits into two paths, as seen in Fig. 3. The first of them is that the terminal nitrogen atom of N_2O approaches the $Pt_{(3)}$ center, leading to the ^{4}IM5 formed, where the $Pt_{(3)}$–N distance is 1.959 Å. The other route is that the terminal nitrogen atom coordinates to $Pt_{(7)}$, namely intermediate ^{4}IM10, which is only 0.2 kcal mol^{-1} higher than its isomer ^{4}IM5. In order to simplify the analysis, the two pathways are represented as Path 1 and Path 2, respectively. From Fig. 3, Path 1 is indicated by the red lines and the blue lines for Path 2. Corresponding to the doublet reaction is high energy pathway, to save space, the optimized structures and energies are shown in Supporting Information (see Table S2). Once the ^{4}IM5 (or ^{4}IM10) intermediate is formed, the following step involves a geometry rearrangement process via ^{4}TS3 (or ^{4}TS5), which has an activation barrier of 7.1 kcal/mol and is exothermic by 4.6 kcal/mol for Path 1.

3.3 Mechanism of the $Pt_4^{+/-} + N_2O \rightarrow Pt_4O^{+/-} + N_2$ reactions

3.3.1 Analysis of activation strain model for the N–O bond cleavage of the transition states

As shown in Fig. 2, for $Pt_4^+ + N_2O$ system, with respect to the quartet state pathway, the intermediate ^{4}IM2 can be formed via the transition state ^{4}TS1. The latter ^{4}TS1 has a feature of partially broken N–O bond (1.6284Å), in which the activation barrier is 40.1 kcal/mol relative to ^{4}IM1. ^{4}TS1 is characterized as a transition state (TS) by one imaginary frequency of 689.6i cm^{-1}, and the vibrational vector corresponds to the expected components of the reaction coordinate, i.e., breaking of the N–O bond. The reaction on the doublet potential energy surface follows similar mechanisms with the quartet state. The intermediate ^{2}IM2 can be formed via the transition state ^{2}TS1 with a reaction barrier of 41.8 kcal/mol. As for the $Pt_4^- + N_2O$ system, the reaction pathways are shown in Fig. 3. This step is strongly exothermic by 50.2 kcal/mol and has a small reaction barrier of 2.6 kcal/mol for Path 1, while Path 2 is almost a non-barrier (about 0.1 kcal/mol) process. A pronounced difference compared with the $Pt_4^+ + N_2O$ system is that it has a low activation barrier of the N–O cleavage transition state, which may be lead to the high efficiency. In other words, Pt_4^- anion assistance, as mentioned above, lowers the reaction barrier for the N–O cleavage.

In order to understand the factors controlling of the N–O cleavage processes, the energies to distort reactants to the transition state geometry (the distortion energy) and the energy of interaction between these distorted reactants (the interaction energy) were analyzed. Such an analysis is also known as the activation strain model. It is related to the deformation/interaction method developed by Morokuma et al. [36, 37], which has been elaborated and applied to some systems. Thus, the activation energy ($\Delta E^{\neq}$) is decomposed into the distortion energies ($\Delta E^{\neq}_{\text{dist}}$, require to distort the reactants into the TS geometry) and the stabilizing transition state (TS) interaction energies ($\Delta E^{\neq}_{\text{int}}$, gained upon allowing the distorted fragments to interact), namely

$$\Delta E^{\neq} = \Delta E^{\neq}_{\text{dist}} + \Delta E^{\neq}_{\text{int}}$$

$$\Delta E^{\neq}_{\text{dist}} = \Delta E^{\neq}_{\text{dist}}(\text{Pt}_4) + \Delta E^{\neq}_{\text{dist}}(\text{N}_2\text{O})$$

These are shown schematically in Fig. 5. The calculated results are summarized in Table 1.

Interestingly, the activation distortion energies ($\Delta E^{\neq}_{\text{dist}}$) fluctuate much less and, in fact, adopt values that for each type of bond are in a characteristic range (see Table 1). The lowering of the activation barriers through Pt_4^- anion assistance is caused by the TS interaction $\Delta E^{\neq}_{\text{int}}$ becoming more stabilizing. For example, going from ^{4}TS1 to ^{4}TS4 (or ^{4}TS6), the barrier of the N–O bond activation is reduced from 43.4 kcal/mol to −0.7 kcal/mol (or −3.4 kcal/mol) (note that the ^{4}5 or ^{4}IM10 intermediate is the reference point for analysis of the latter two values), the activation distortion energies remain in the same order for N_2O, ca. 71.7–78.2 kcal/mol, and the strength of the TS interaction

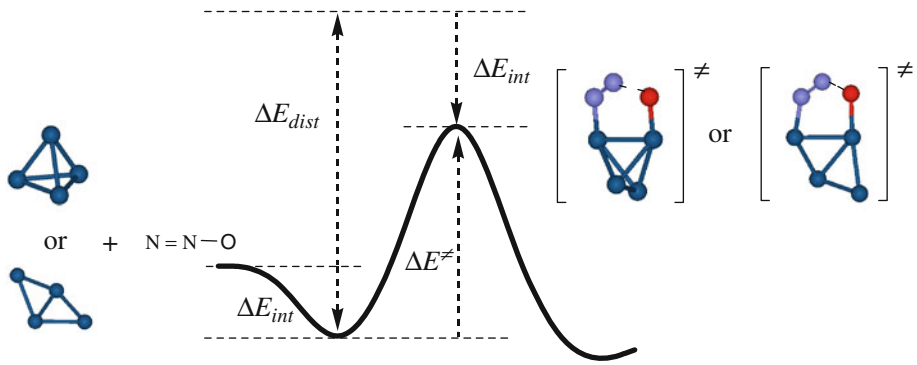

Fig. 5 Distortion/interaction model for the N–O bond cleavage

Table 1 Distortion/interaction analysis of TSs involving ^{4}TS1, Pt_4^-–^{4}TS4, and ^{4}TS6

TS	$\Delta E^{\neq}$	ΔE_{dist}		ΔE_{int}	
		N_2O	Pt_4	TS	Reference point
^{4}TS1	43.42	71.69	4.85	−47.97	−14.85
^{4}TS4	−0.71	78.20	1.72	−95.55	−14.92
^{4}TS6	−3.35	73.01	0.46	−90.67	−13.85

increases from 47.9 kcal/mol in the ^{4}TS1 transition state to 95.6 kcal/mol in the ^{4}TS4 transition state. These TS compounds have large differences in interaction energies, which are strongly linked to the different activation energies. The interaction energies may control the N–O cleavage processes.

Clearly, the distortion energies are related to the relative bond dissociation energies [61], but what controls the interaction energies? We have found that the N_2O π*-LUMO and Pt d HOMO interaction controls the relative interaction energies, which are shown in Fig. 4 (right). Analysis of the frontier molecular orbitals of the N–O cleavage transition states leads to a rationalization of the results obtained. Pt_4^- is an electron-rich d metal cluster. The N–O cleavage TS will thus be stabilized if back-donation is possible. Moreover, this back-donation should be more pronounced as the $HOMO_{Pt}$-$LUMO_{Nitrous\ oxide}$ gap becomes smaller. A charge transfer occurs at the initial intermediate stage of the reaction from Pt_4 to the LUMO of $N_2O(3\pi)$. Population of this orbital, however, bends the molecule, because the optimal state of the N_2O^- ion is bent (with destabilized N–O and N–N bonds). The bending of the N_2O ligand results in a 2.9 eV splitting of the doubly degenerate LUMO (3π orbital, Fig. 4) of N_2O into two lower-energy, nondegenerate π* orbitals. The low-energy LUMO of the bent N_2O ligand can now strongly couple with the occupied $Pt_{(3)}$/$Pt_{(7)}$-localized d-orbitals, forming a back-bond between the N_2O ligand and the Pt_4 cluster and transferring charge from $Pt_{(3)}$/$Pt_{(7)}$ to the N_2O ligand. The HOMO of the Pt_4^+–^{4}TS1 transition state has 66.7% π* LUMO(N_2O) character, with 3d orbital contributions of 14.1% from $Pt_{(3)}$ and 12.3% from $Pt_{(7)}$ (see Fig. 4), while HOMO has 81.5% π* LUMO(N_2O) character, with 3d orbital contributions of 10.7% from $Pt_{(3)}$ and 7.7% from $Pt_{(7)}$ for ^{4}TS4. This very significant back-bonding interaction is further confirmed by the natural population analysis, which indicates a large negative charge (−0.79 e) of the N_2O ligand in the ^{4}TS4 transition state. For the ^{4}TS1 transition state, a negative charge of the N_2O ligand is only −0.22 e. As a result of this significant back-bonding, the stronger $Pt_{(3)}$–N and $Pt_{(7)}$–O interactions and weaker N–O and N–N bonds compensate the large deformation energy of the N_2O ligand, and the resulting ^{4}TS4 transition state is more stable than the ^{4}TS1 transition state.

3.3.2 *Analysis of spin density (ρ) and atomic charge (q) along the quartet Pt_4^+–^{4}TS1 and Pt_4^-–^{4}TS2 IRC pathways*

To emphasize the importance of charge transfer, we plotted the spin density (ρ) and atomic charge (q) of the reacting atoms with respect to the reaction coordinate in Supporting Information (see Figures S2 and S3). Mulliken population analysis indicates that the electronic rearrangements at the early stages after the transition state are a key factor of the N–O bond cleavage. The difference of the charge values may significantly impact on the reaction mechanism. For example, the charges of the N_2O molecule are −0.99 e for the ^{4}TS4 system and −0.32 e for the ^{4}TS1 system at IRC = −5.3 a.u. step, respectively. Obviously, the charge transfer of the ^{4}TS4 system is much stronger than that of the ^{4}TS1 system, which leads to the different reaction mechanism [62]. Our calculation revealed that the electron transfer from Pt_4^- toward the N_2O molecule yields a N_2O^- ion (Mulliken population analysis indicated ca. 0.79–0.99 e transferred to N_2O, and the bending of the molecule also shows this fact). The dissociation of a bent N_2O^-, however, follows this spin-conserving route: $N_2O(^2A') \rightarrow N_2(^1\sum_g^+) + O^-\ (^2P)$. In this way, the dissociation of N_2O is directly coupled to the Pt_4O^- formation without barrier coming from surface crossings. However, for the ^{4}TS1 system, the diabatic (spin conserving) dissociation of N_2O: $N_2O(^1\sum^+) \rightarrow N_2(^1\sum_g^+) + O(^1D)$ is unreactive, excited state oxygen atom, well above the adiabatic $N_2(^1\sum_g^+) + O(^3P)$ surface due to the weaker charge transfer. It has been therefore assumed that a hopping from the $O(^1D)$ surface to the $O(^3P)$ surface is partly responsible for the slow reaction rate. Namely, the reaction may go through the intersection of the quartet and doublet surfaces.

3.3.3 *Analysis of surface-crossing behavior and spin–orbit coupling (SOC) along the Pt_4^+–^{4}TS1 IRC pathway*

Before discussion of the SOC influence on the process of the N–O bond cleavage, we first tried to locate the crossing points between the quartet and doublet surfaces along the ^{4}TS1 IRC pathway because the intermediate complex in doublet state, ^{2}IM2, will be formed from the intermediate in quartet state, ^{4}IM1 via the transition state ^{4}TS1 with the N–O bond broken. At least, a crossing point and spin inversion process may be taken place in the reaction pathway. Thus, we performed single-point computation of the quartet state as a function of the structural change along the IRC of the doublet state (from the transition state ^{4}TS1 to complex ^{4}IM2). This method was suggested by

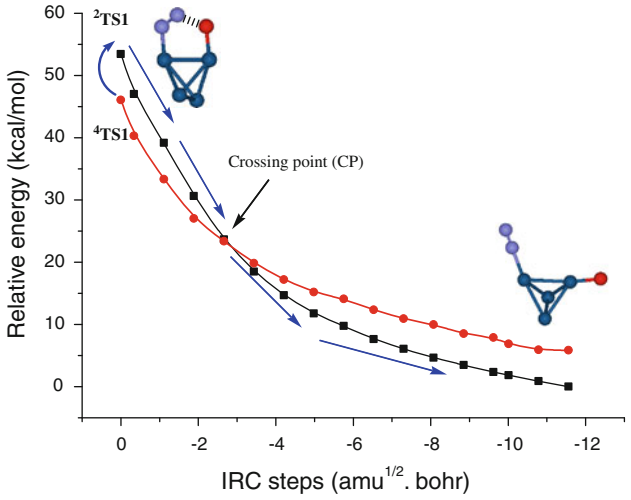

Fig. 6 Potential energies curve-crossing diagram for the different spin-state PESs along the doublet ^{2}TS1 IRC at the B3LYP/6-311++G(d, p)+SDD level

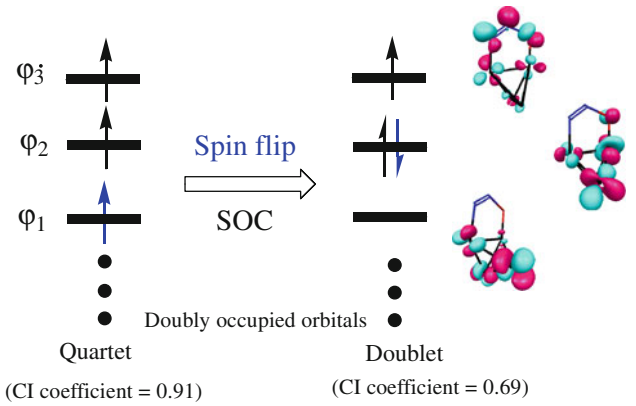

Fig. 7 Schematic illustration of the required electronic structure change for the quartet → doublet transformation. In order to save space, the double-occupied non-active orbitals are omitted

Yoshizawa [49] for approximately locating the crossing points of two PESs with different multiplicities. The calculated results are shown in Fig. 6, and CP is located at IRC = −2.66 a.u., in which the dissociating N–O bond distance is 1.9828 Å and the forming Pt–O bond distance is 1.8557 Å. It is an upper bound of the energy of the true MECP obtained by computing single-point energies. The quartet and the doublet potential energy surfaces can begin to touch at this point because the IRC valley of the quartet state still lies below that of the doublet state in this region of reaction pathway. One mechanism is the spin hopping that is easily taken place at the CP point because of the same both energies and geometries. Then, the reaction system will access to a lower energy pathway by changing its spin multiplicities via the CP point. However, it is noted that the likelihood of such a crossover seems significant in view of the fact that the spin-state surfaces are so close and cross from ^{4}TS1 to CP (see Fig. 6). As such, one may think about another mechanistic scenario [63] that is depicted in Fig. 6 (as shown schematically by the blue arrows), a change in the geometry of the quartet ^{4}TS1 in the direction of the doublet ^{2}TS1, causes crossing between the two states. Thereafter, the reaction can proceed on the doublet surface or bifurcate again to the quartet surface. What kind of mechanism was happened, which will depend on the magnitude of the transition probability? But among the factors that affect the magnitude of the transition probability is the SOC interaction between the states. Therefore, the strength of SOC and the energy gap are keys to understanding mechanism. Let us then discuss the SOC interaction.

The ROHF orbitals for the construction of the quartet and doublet CASCI wave functions to be used in the SOC evaluation have been generated in the ^{4}TS1 region by the quartet ROHF calculation, at least three active orbitals, as depicted in Fig. 7 (in order to save space, the double-occupied non-active orbitals are omitted). Interestingly, the ^{4}TS1 region showed significant multireference character for the doublet state. At the CAS (9, 7) level, the dominant determinants of the MCSCF wave functions have configuration interaction (CI) coefficients of 0.91 and 0.06 for the quartet and 0.69, 0.46, and 0.44 for the doublet state. Thus, the permissible approximation of the quartet wave function by a single configuration (0.91) enables us to analyze the SOC matrix element in a simple formula. For the doublet state, although the "open-shell" configuration $^2\varphi_1\varphi_2\varphi_3$ shares a great proportion (the CI coefficient is about 0.46 or 0.44) in the doublet ground configurations, the direct conversion from the quartet reference state is forbidden because of incompatibility of spin inversion for the two electronic states. Therefore, the $^2\varphi_3$ configuration is the dominant configuration with the weight of about 0.69 in the ^{4}TS1 region. Nonzero elements of the k-components ($k = x$, y, and z) of the SOC matrix, $\langle {}^4\psi(M_s)|\hat{H}_{SO}|{}^2\psi(M_s)\rangle_k$, are always proportional to the function, F_k, as given in Eq. 3.

$$F_k = 2^{-1/2}\lambda\langle\phi_1|\hat{h}_k|\phi_2\rangle\left(\hat{h}_k = \frac{\alpha^2}{2}\sum_A \frac{Z_A\hat{l}_A^k}{r_A^3}\right) \quad (3)$$

where λ is the CI mixing coefficient. As we previous determined [11], to a rough approximation, the SOC matrix element will be determined by the variation of four main factors: the delocalization of the MO's as accounted for by the MO coefficient term; the resulting angular momentum points in the positive direction is attributed to the direction of the orbitals rotation; the ROHF configuration coefficient (λ) of the doublet state, and the "heavy atom" effect.

The one-electron SOC value calculated is 677.9 cm^{-1} in the ^{4}TS1 region. The notably larger SOC is easy to understand, as can be see from Fig. 7, since during spin

flip, the electron in the φ_1 orbital in the quartet state shifts to the φ_2 orbital, the SOC between the states would be maximized when both orbitals are localized on Pt. While the φ_1 orbital is fairly localized, the φ_2 orbital is delocalized toward the adjacent O atom of the ligand. Moreover, for a transition metal complex where there are a number of near-degenerate states due to close lying metal d-orbitals. The SOC value is large enough to contribute to the spin transition; we expect that the quartet to doublet state transition should occur efficiently near the ^{4}TS1. We also noted that ^{4}TS1 is late transition state compared with ^{2}TS1, and the spin flip will occur in the energy decrease stage of the doublet surface, which also leads to the high magnitude of the transition probability. In addition, the spin flip will lead to a small increase in the barrier height of ^{4}TS1 from 40.1 to 47.3 kcal/mol at the B3LYP/6-31++G(d, p)+LanL2DZ. As for the CP region, the SOC value is decreased to 476.1 cm^{-1}, which is attributed to the φ_2 orbital is further delocalized toward the adjacent O atom and the r_A^{-3} dependence. These results indicate that the reaction of the N–O bond cleavage will be occurred along the direction of the blue arrows, as shown in Fig. 7. Not only will the reaction overcome spin-change-induced barrier [64] (ca. 7 kcal/mol) but also overcome adiabatic barrier (ca. 40.1 kcal/mol), which is regarded as the rate-determining step in the entire reactions. Thus, we conclude that the lack of a thermodynamic driving force is an important factor contributing to the low efficiency of the reaction system.

3.4 Mechanism of the $Pt_4O^{+/-} + CO \rightarrow Pt_4^{+/-} + CO_2$ reactions

The calculated potential energy profiles for the quartet and doublet states are shown in Figs. 2 and 3. Corresponding geometries are depicted in Fig. 1. As can been seen Fig. 2, once the N–O bond is broken, the following steps involve the dissociation of the N_2 molecule, combination of CO molecule to form $[OPt_4CO]^+$, and finally dissociation of CO_2. This step of reaction is the coordination of the CO molecule to the Pt center of Pt_4O^+, producing $[OPt_4CO]^+$ (^{4}IM4 or ^{2}IM4) complex. In accordance with our studies, the quartet state of ^{4}IM4 is calculated to be more stable than the doublet state, ^{2}IM4, by about 6.8 kcal mol^{-1}. The C–O cleavage transition state, ^{4}TS2 (or ^{2}TS2), has only one imaginary frequency 579.9i cm^{-1} (or 462.1i cm^{-1}) corresponding to the C–O stretching reaction coordinate. These processes are thermodynamically favorable and very exothermic by 71.8 kcal/mol in the quartet state and 62.9 kcal/mol in the doublet state relative to ^{2}IM3 + N_2, respectively (see Fig. 2).

Unfortunately, the $[OPt_4CO]^-$ coordination intermediates cannot be formed on the doublet and quartet potential energy surfaces for the Pt_4O^- + CO system, while directly form the stable intermediates $[Pt_4CO_2]^-$, ^{4}IM9 (or ^{4}IM14). Figure 3 shows that introduction of carbon monoxide in the reaction environment yields the $[Pt_4CO_2]^-$ adducts, ^{4}IM9 (or ^{4}IM14), lying 46.2 kcal/mol and 40.8 kcal/mol below ^{4}IM8 + N_2, respectively. By contrast, Path 2 (indicated by the blue lines) is the low energy pathway for the $Pt_4O^- + CO \rightarrow Pt_4^- + CO_2$ process, but it is the high energy pathway for $Pt_4^- + N_2O$ reaction.

4 Conclusions

The title reactions have been studied using theoretical calculations. All structures of the quartet and doublet potential energy surfaces are determined and characterized at the DFT-B3LYP level. To obtain a physical understanding of how anion assistance works, we have analyzed the three model reactions using the activation strain model in which the activation energy ($\Delta E^{\neq}$) is decomposed into the distortion energies ($\Delta E^{\neq}_{\text{dist}}$) and the stabilizing transition state (TS) interaction energies ($\Delta E^{\neq}_{\text{int}}$), namely $\Delta E^{\neq} = \Delta E^{\neq}_{\text{dist}} + \Delta E^{\neq}_{\text{int}}$. Crossing point between the potential energy surfaces is located using Yoshizawa's method, and possible spin inversion process is discussed by means of spin–orbit coupling (SOC) calculations.

As a result, the effect of Pt_4^- anion assistance is analyzed using the activation strain model in which the activation energy ($\Delta E^{\neq}$) is decomposed into the distortion energies ($\Delta E^{\neq}_{\text{dist}}$) and the stabilizing transition state (TS) interaction energies ($\Delta E^{\neq}_{\text{int}}$), namely $\Delta E^{\neq} = \Delta E^{\neq}_{\text{dist}} + \Delta E^{\neq}_{\text{int}}$. The lowering of activation barriers through Pt_4^- anion assistance is caused by the TS interaction $\Delta E^{\neq}_{\text{int}}$ (−90.7 to −95.6 kcal/mol) becoming more stabilizing. What controls the interaction energies? We have found that the N_2O π*-LUMO and Pt d HOMO interaction controls the relative interaction energies, which demonstrated that electron transfer from the $Pt_4^{+/-}$ cluster to N_2O is an essential ingredient of the N–O bond cleavage, but the strength of the charge transfer has significantly impact on the reaction mechanism.

For the Pt_4^+ cation system, compared with the Pt_4^- anion, the strength of the charge transfer is weaker, which leads to the diabatic (spin conserving) dissociation of N_2O: $N_2O(^1\sum^+) \rightarrow N_2(^1\sum_g^+) + O(^1D)$. Namely, the reaction may go through the intersection of the quartet and doublet surfaces. The quartet to doublet state transition should occur efficiently near the ^{4}TS1 due to the larger one-electron SOC value calculated of 677.9 cm^{-1}.Thus, not only will the reaction overcome spin-change-induced barrier (ca. 7 kcal/mol) but also overcome adiabatic barrier (ca.

40.1 kcal/mol), which is regarded as the rate-determining step in the entire reactions. Therefore, the lack of a thermodynamic driving force is an important factor contributing to the low efficiency of the reaction system. As for the Pt_4^- anion system, HOMO has 81.5% π^* LUMO(N_2O) character, with 3d orbital contributions of 10.7% from $Pt_{(3)}$ and 7.7% from $Pt_{(7)}$ near the ^{4}TS4 transition state. This very significant back-bonding interaction is further confirmed by the natural population analysis, which indicates a large negative charge (s0.79 e) of the N_2O ligand. This facilitates the bending of the N_2O molecule, and the dissociation of a bent N_2O^- ,however, follows this spin-conserving route: $N_2O(^2A') \rightarrow N_2(^1\sum_g^+) + O^-$ (^{2}P). In this way, the dissociation of N_2O is directly coupled to the Pt_4O^- formation without barrier coming from surface crossings.

Acknowledgments We are grateful to the National Natural Science Foundation of China (Grant No. 20873102), the Ph. D. foundation of the Northwest Normal University, and TianShui Normal University for grant the 'QingLan' talent engineering funds for support of this research.

References

1. Prather RA, Ehhalt DH (2001) In climate change 2001: the scientific basis. In Houghton JT et al (ed) Cambridge University Press, New York
2. Tishchenko O, Nguyen CMT (2004) J Phys Chem A 108:1268
3. Delabie A, Pierloot K (2002) J Phys Chem A 106:5679
4. Wiesenfeid JR, Yuen MJ (1976) Chem Phys Lett 42:293
5. Ritter D, Weisshaar JC (1989) J Phys Chem 93:1576
6. Ritter D, Weisshaar JC (1990) J Phys Chem 94:4907
7. Chen P, Cabrito I, Moura JJG, Moura I, Solomom EI (2002) J Am Chem Soc 124:10497
8. Gorelsky SI, Ghosh S, Solomon EI (2006) J Am Chem Soc 128:278
9. Chiodo S, Rondinelli F, Russo N, Toscano M (2008) J Chem Theory Comput 4:316
10. MeClean RE, Campbell ML, Goodwin RH (1996) J Phys Chem 100:751
11. Lv LL, Wang YC, Liu HW, Wang Q (2010) Theor Chem Acc 127:507
12. Delabie A, Vinckier C, Flock M, Pierloot K (2001) J Phys Chem A 105:5479
13. Lv LL, Liu XW, Wang YC (2006) J Mol Struct: THEOCHEM 774:59
14. Lv LL, Wang YC (2005) J Mol Struct: THEOCHEM 724:185
15. Stirling A (2002) J Am Chem Soc 124:4058
16. Parent DC, Anderson SL (1992) Chem Rev 92:1541
17. Brönstrup M, Schröder D, Kretzschmar I, Schwarz H, Harvey JN (2001) J Am Chem Soc 123:142
18. Reveles JU, Johnson GE, Khanna SN, Castleman AW Jr (2010) J Phys Chem C 114:5438
19. Riley SJ (1994) In clusters of atoms and molecules II. In H. Haberland (ed.). Springer, Berlin, p 221
20. Blagojevic V, Orlova G, Bohme DK (2005) J Am Chem Soc 127:3545
21. Böhme DK, Schwarz H (2005) Angew Chem Int Ed 44:2336
22. Kappes MM, Staley RH (1981) J Am Chem Soc 103:1286
23. Rondinelli F, Russo N, Toscano M (2008) J Chem Theory Comput 4:1886
24. Wang YC, Wang QY, Geng ZY, Si YB, Zhang JH (2008) Chem Phys Lett 460:13
25. Koszinowski K, Schröder D, Schwarz H (2003) J Phys Chem A 107:4999
26. Shi Y, Ervin KM (1998) J Chem Phys 108:1757
27. Siu CK, Reitmeier SJ, Balteanu I, Bondybey VE, Beyer MK (2007) Eur Phys J D 43:189
28. Armentrout PB (1990) Annu Rev Phys Chem 41:313
29. Armentrout PB (1991) Science 251:175
30. Rue C, Armentrout PB (1999) J Chem Phys 110:7858
31. Fiedler A, Schröder D, Shaik S, Schwarz H (1994) J Am Chem Soc 116:10734
32. Shaik S, Danovich D, Fiedler A, Schröder D, Schwarz H (1995) Helv Chim Acta 78:1393
33. Hirao H, Kumar D, Que L, Shaik S (2006) J Am Chem Soc 128:8590
34. Schröder D, Shaik S, Schwarz H (2000) Acc Chem Res 33:139
35. Harvey JN, Poli R, Smith KM (2003) Coord Chem Rev 238–239:347
36. Diefenbach A, Theodoor de Jong G, Bickelhaupt FM (2005) J Chem Theory Comput 286:1
37. Morokum K (1971) J Chem Phys 55:1236
38. Frisch MJ et al (2003) Gaussian 03 (Revision-E.01). Gaussian Inc., Pittsburgh PA
39. Frisch MJ, Pople JA, Binkley JS (1984) J Chem Phys 80:3265
40. Hay PJ, Wadt WR (1985) J Chem Phys 82:270
41. Wadt WR, Hay PJ (1985) J Chem Phys 82:284
42. Cao XY, Dolg M (2001) J Chem Phys 115:7348
43. Davidson ER (2000) Chem Rev 100:351
44. Aschi M, Bronstrup M, Diefenbach M, Harvey JN, Schroder D, Schwarz H (1998) Angew Chem Int Ed 37:829
45. Zhang D, Liu CB, Bian WS (2003) J Phys Chem A 107:8955
46. Wang YC, Zhang JH, Geng ZY (2007) Chem Phys Lett 446:8
47. Liu ZY, Wang YC, Geng ZY, Yang XY (2006) Chem Phys Lett 431:223
48. Wang YC, Wang Q, Geng ZY, Lv LL, Si YB (2009) J Phys Chem A 113:13808
49. Yoshizawa K, Shiota Y, Yamabe T (1999) J Chem Phys 111:538
50. Lv LL, Wang YC, Geng ZY, Si YB, Wang Q, Liu HW (2009) Organometallics 28:6160
51. Glendenin ED, Badenhoop JK, Reed AE, Carpenter JE, Bohmann JA, Morales CM, Weinhold F (2001) NBO 5.0. Theoretical Chemistry Institute, University of Wisconsin, Madison
52. Danovich D, Marian CM, Neuheuser T, Peyerimhoff SD, Shaik S (1998) J Phys Chem A 102:5923
53. Isobe H, Yamanaka S, Kuramitsu S, Yamaguchi K (2008) J Am Chem Soc 130:132
54. Koseki S, Schmidt MW, Gordon MS (1992) J Phys Chem 96:10768
55. Salem L, Rowland C (1972) Angew Chem Intern Edit 11:92
56. Schmide MW, Baldridge KK, Boatz JA, Elbert ST, Gordon MS, Jensen S, Koseki N, Matsunaga KA, Nguyen SJ, Su T, Windus LM, Dupuis JH, Montgomery JA (1993) J Comput Chem 14:1347
57. Peyerimhoff SD, Buenker RJ (1968) J Chem Phys 49:2473
58. Hwang DY, Mebel AM (2000) Chem Phys 259:89
59. Nnčák ML, Cao Y, Höckendorf RF, Beyer MK, Zahradník R, Schwarz H (2009) Chem Eur J 15:8465
60. Fukui K (1981) Acc Chem Res 14:363
61. Schoenebeck F, Houk KN (2010) J Am Chem Soc 132:2496
62. Stirling A (1998) J Phys Chem A 102:6565
63. Hirao H, Kumar D, Que JL, Shaik S (2006) J Am Chem Soc 128:8590
64. Poli R, Harvey JN (2003) Chem Soc Rev 32:1